Ensemble inequivalence in the Blume-Emery-Griffiths model near a fourth-order critical point

V. V. Prasad,[1,*] Alessandro Campa,[2] David Mukamel,[1] and Stefano Ruffo[3]

[1]*Department of Physics of Complex Systems, Weizmann Institute of Science, Rehovot 7610001, Israel*

[2]*National Center for Radiation Protection and Computational Physics, Istituto Superiore di Sanità, Viale Regina Elena 299, 00161 Rome, Italy*

[3]*SISSA, INFN and ISC-CNR, Via Bonomea 265, I-34136 Trieste, Italy*

(Received 21 August 2019; published 22 November 2019)

The canonical phase diagram of the Blume-Emery-Griffiths model with infinite-range interactions is known to exhibit a fourth-order critical point at some negative value of the biquadratic interaction $K < 0$. Here we study the microcanonical phase diagram of this model for $K < 0$, extending previous studies which were restricted to positive K. A fourth-order critical point is found to exist at coupling parameters which are different from those of the canonical ensemble. The microcanonical phase diagram of the model close to the fourth-order critical point is studied in detail revealing some distinct features from the canonical counterpart.

DOI: 10.1103/PhysRevE.100.052135

I. INTRODUCTION

Long-range interacting systems have gained considerable attention, due to their unusual characteristics when compared with the widely studied systems with short-range interactions [1,2]. By long-range interacting systems, one refers to cases where the two-body interaction potential between degrees of freedom decays algebraically with the distance r as $1/r^{d+\sigma}$, where d is the spatial dimension and $\sigma \leqslant 0$. Such systems, for which the energy and other thermodynamic potentials are nonadditive, are rather widely spread in nature, including self-gravitating systems ($d = 3$, $\sigma = -2$) [3,4], interacting geophysical vortices ($d = 2$ and logarithmic interaction) [3], dipolar interactions in ferroelectrics and ferromagnets($d = 3$, $\sigma = 0$) [5], and plasmas [6] to name a few. The case $\sigma = -d$ corresponds to infinite-range, mean-field interaction, which has conveniently been used to study various features of long-range interacting systems.

The nonadditive nature of thermodynamic quantities in long-range systems makes them rather different from the more commonly studied systems with short-range interactions, resulting in a number of nontrivial features such as inequivalence of different ensembles [7,8]. For example, one finds that in these systems the entropy need not be a concave function of energy, which implies a negative specific heat in the microcanonical ensemble. This is in contrast with what is obtained in the canonical ensemble. In addition at first-order phase transitions the temperature displays a discontinuity in the microcanonical ensemble, a feature which is clearly absent in the canonical ensemble. Similar features are found when grand-canonical and canonical ensembles are compared [9]. The lack of additivity results in the presence of nonconvex domains in the parameter space of accessible thermodynamic variables and in breaking of ergodicity [10,11]. Various other interesting effects have been predicted in the relaxation of certain long-range systems to their final equilibrium state, where the system approaches intermediate long-lived "quasistationary states" before reaching equilibrium [12–15].

A simple paradigmatic model in which properties of systems with long-range interactions have been studied and ensemble inequivalence has been demonstrated is the Blume-Emery-Griffiths (BEG) model, introduced to study the phase separation and transition to superfluidity in $He^3 - He^4$ mixtures [16], which was later generalized and used for studying generic two-component fluid mixtures [17,18]. This is a spin-1 lattice model with both bilinear and biquadratic spin-spin interactions. In the case of infinite-range interactions, where every spin interacts with every other spin with the same coupling constants ($\sigma = -d$), the Hamiltonian of the model can be represented as

$$H = \Delta \sum_{i=1}^{N} S_i^2 - \frac{J}{2N}\left(\sum_{i=1}^{N} S_i\right)^2 - \frac{K}{2N}\left(\sum_{i=1}^{N} S_i^2\right)^2, \quad (1)$$

where each spin S_i takes one of the values $\{-1, 0, 1\}$. The parameter Δ controls the energy difference between the ferromagnetic ($S_i = \pm 1$) and the paramagnetic ($S_i = 0$) states, $J > 0$ is a ferromagnetic coupling and K is a biquadratic coupling which could have either sign. Even though each spin interacts with every other spin, the scaling J/N and K/N makes the energy extensive (although not additive). Without loss of generality one may take $J = 1$.

The canonical phase diagram of the model (1) has been shown to display unique features at different domains of model parameters [16–20]. For fixed $K \geqslant 0$ the (Δ, T) phase diagram exhibits a ferromagnetic ordered phase at small values of T and Δ and a paramagnetic disordered phase otherwise. However, some qualitative features of the phase diagram are modified as K increases, as shown in Fig. 1. At small K the transition line between the two phases changes character from continuous (solid black) to first-order (dashed red) at a tricritical point (green dot). At higher values of K [21], another first-order line emerges, separating two disordered phases. The two first-order lines meet at a triple point

*Corresponding author: prasad.vv@weizmann.ac.il

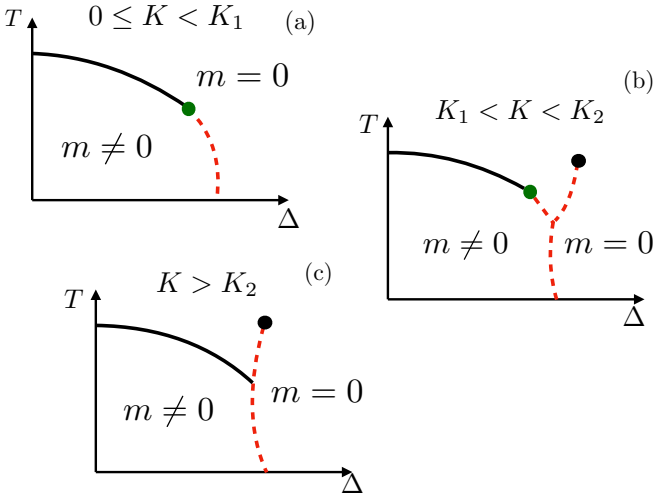

FIG. 1. Schematic plot showing the canonical phase diagram in the (Δ, T) plane for different domains of $K \geqslant 0$. Plot (a) corresponds to the range $0 < K < K_1 \approx 2.775$, where the transition line separating the ferromagnetic (ordered, $m \neq 0$ [see Eq. (3) for the definition of m]) and paramagnetic (disordered, $m = 0$) phase is composed of continuous (solid black) and first-order (dashed red) line segments meeting at the tricritical point (green dot). Plot (b) is for $2.775 \approx K_1 < K < K_2 \approx 3.801$, where in addition to the features described for $K < K_1$, the first-order line branches at a triple point into the disordered phase, indicating a transition between two disordered phases with different quadrupole moment. This branch terminates at a critical point (black dot). Plot (c) is for $K > K_2$, where the second- and first-order lines join at a critical end point rather than at a tricritical one.

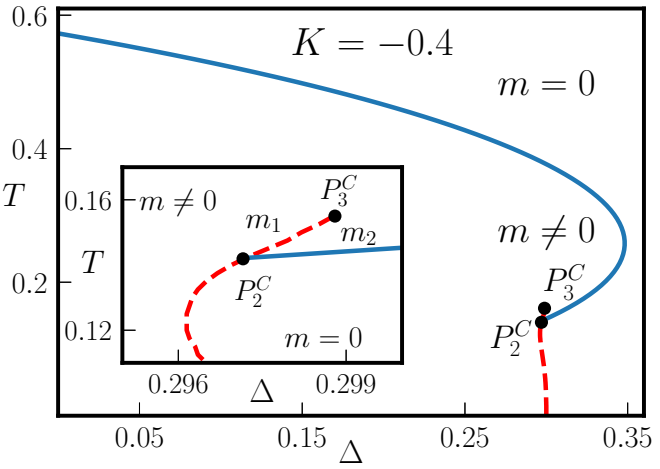

FIG. 2. The canonical phase diagram in the (Δ, T) plane for $K = -0.4$. Here the continuous transition line (solid blue) meets the first-order line (dashed red) at a critical end point denoted by P_2^C ($\Delta \approx 0.2972$, $T \approx 0.1412$). The first-order line extends into the ordered phase, where it marks a transition between two ordered phases with different values of m and q, and terminates at the critical point P_3^C ($\Delta \approx 0.29873$, $T \approx 0.1544$). The zoomed-in phase diagram close to this transition is plotted in the inset.

where the two disordered phases coexist with the ordered one [see Fig. 1(b)]. For even larger K values, the tricritical point becomes a critical end point [see Fig. 1(c)] and the continuous branch of the transition line terminates at the intersection with the first-order line.

The canonical phase diagram for $K < 0$ has also been addressed [18,20]. It has been shown that while at small K the phase diagram is qualitatively similar to the $K = 0$ one (with first and second-order lines joining at a tricritical point), at some particular value of K the tricritical point becomes a fourth-order one. Beyond that value, the phase diagram becomes rather different from that of positive K. While the second-order line terminates at the first-order one at a critical end point (as in the $K > 0$ regime), the first-order line enters into the ordered phase separating two distinct ferromagnetically ordered phases (see Fig. 2). This phase diagram holds, schematically, for a range of values of negative K.

The microcanonical phase diagram was studied for the model for $K = 0$ [22] and for $K > 0$ [21], illustrating the inequivalence between the two ensembles. It has been demonstrated that while the two ensembles have a common critical line at small values of K, the two ensembles yield distinct phase diagrams in the region where the canonical transition is first-order. In particular the microcanonical tricritical point is located at a different point in the phase space of the model. Detailed studies of the phase diagram in the vicinity of the tricritical point show that the microcanonical first-order line does not coincide with its canonical counterpart, and that it involves temperature discontinuity, which is of course missing in the canonical treatment. Furthermore, analysis of large positive values of K reveals a wealth of different features in the phase diagrams of the two ensembles [21].

In the present paper we extend the study of the microcanonical phase diagram of the infinite range BEG model to negative values of the parameter K where a fourth-order critical point has been found in the canonical phase diagram. As is usually the case, a high-order critical point determines the topological features of the phase diagram around it and the way the various phase transition manifolds join together. These topological features tend to persist in quite a broad range of the model parameters, making a study of this point of particular interest. The fact that the canonical phase diagram of this model exhibits a fourth-order critical point at some negative value of K suggests that such a point may also exist in the microcanonical phase diagram as well, which would enable one to make a detailed comparison between the phase diagrams of the model obtained in the two ensembles. We find that indeed the microcanonical phase diagram exhibits a fourth-order critical point at negative K, located at a different point in phase space as compared with the canonical one. We analyze the global features of the microcanonical phase diagram and discuss the way the inequivalence between the two ensembles is manifested in this parameter region.

The rest of the paper is as follows: A brief outline of the analysis of BEG model in the canonical ensemble is presented in Sec. II, which allows us to display the phase diagram in the relevant region of the parameter space. The analysis is carried out for $K < 0$, for which the fourth-order transition point is present. In Sec. III the microcanonical analysis of the model is presented, and the fourth-order point in this ensemble is identified. In Sec. IV we discuss in detail the

microcanonical phase diagram around the fourth-order critical point. Concluding remarks are given in Sec. V.

II. CANONICAL PHASE DIAGRAM

In the following, we briefly outline the derivation of the canonical phase diagram for negative K, where a fourth-order critical point is found to be present. Note that in nonadditive systems, such as the one considered in this paper, the canonical ensemble cannot be simply derived from the microcanonical one. For a discussion of this point see Refs. [23,24]. Here we consider the partition function of the system,

$$Z(\beta = 1/T, N) = \sum_{\{S_i\}} e^{-\beta H}, \tag{2}$$

where H is as given in Eq. (1), with the Boltzmann constant $k_B = 1$. Let

$$m = \sum_{i=1}^{N} S_i/N \quad \text{and} \quad q = \sum_{i=1}^{N} S_i^2/N \tag{3}$$

be the magnetization m and quadrupole moment q order parameters, respectively. The partition function can be calculated by converting the right-hand side of Eq. (2) into an integral using the Hubbard-Stratonovich transformation. Making use of the Gaussian identity,

$$e^{ab^2} = \sqrt{\frac{|a|}{\pi}} \int_{-\infty}^{\infty} dx\, e^{-|a|x^2 + 2sabx} \tag{4}$$

where $s = 1$ for $a > 0$ and $s = i$ (the imaginary unit) for $a < 0$, one can represent the partition function as

$$Z(\beta, N) = \frac{N\beta\sqrt{-K}}{2\pi} \sum_{\{S_i\}} e^{-\beta N \Delta q} \times \int_{-\infty}^{\infty}\int_{-\infty}^{\infty} dx\, dy\, e^{-\frac{\beta N}{2}x^2 + \frac{\beta N K}{2}y^2 + \beta N m x + \beta N K q i y}, \tag{5}$$

where x and y are the corresponding auxiliary fields. We point out that in this paper we are considering only positive temperatures, although this model, where the energy is upper bounded, allows also negative temperatures in the microcanonical ensemble [21]. Therefore in the following it is always $\beta > 0$.

Performing the sum over $\{S_i\}$ results in

$$Z(\beta, N) = \frac{N\beta\sqrt{-K}}{2\pi} \int_{-\infty}^{\infty}\int_{-\infty}^{\infty} dx\, dy e^{-\beta N \tilde{f}(\beta,x,y)}, \tag{6}$$

where

$$\beta\tilde{f}(\beta, x, y) = \frac{\beta}{2}(x^2 - Ky^2) - \ln[1 + 2e^{-\beta\Delta + \beta K i y}\cosh(\beta x)]. \tag{7}$$

The integration can be done using a saddle point analysis in terms of the variables x and y. Note that the values x and iy which minimize $\beta\tilde{f}(\beta, x, y)$ correspond respectively to the equilibrium magnetization m and the quadrupole moment q, where the minimizing value of y is purely imaginary. At the saddle point one obtains

$$x = \frac{2\sinh\beta x}{e^{\beta\Delta - i\beta K y} + 2\cosh\beta x}, \tag{8}$$

$$iy = \frac{2\cosh\beta x}{e^{\beta\Delta - i\beta K y} + 2\cosh\beta x}. \tag{9}$$

Furthermore, for a nonzero magnetization (which corresponds to $x \neq 0$) the above relations also lead to the expression

$$iy = x\coth\beta x. \tag{10}$$

One will find these relations to be useful when characterizing the phase diagram, as explained below.

To obtain the critical line one expresses y in terms of x using Eq. (10) and expands the free energy $\tilde{f}(\beta, x, y)$ about the paramagnetic solution $x = 0$ and $iy = 1/\beta$ [see Eqs. (8) and (10)] in powers of x,

$$\beta f(\beta, x, y(x)) = \beta f_o + A_c x^2 + B_c x^4 + C_c x^6 + D_c x^8 \cdots, \tag{11}$$

where f_0 is the free energy value at $x = 0$,

$$A_c = \frac{\beta(3 + 2K)}{6}\left[1 - \frac{2\beta}{2 + e^{\beta\Delta - K}}\right], \tag{12}$$

and B_c, C_c, and D_c are given by more complicated expressions of β, Δ, and K which are not displayed here. The critical surface is obtained at $A_c = 0$, yielding

$$\beta = 1 + \tfrac{1}{2}e^{\beta\Delta - K}. \tag{13}$$

The critical surface represents a locally stable solution as long as B_c is positive. On the critical surface [Eq. (13)] the coefficient B_c takes the form

$$B_c = \frac{\beta^2}{72}(2K + 3)[(2K + 3) - \beta(2K + 1)]. \tag{14}$$

Considering $K > -0.5$, the region where the fourth-order critical point is located, the critical surface is stable for $(3 + 2K)/(1 + 2K) > \beta$, and it terminates on a tricritical line obtained at $B_c = 0$, namely, at

$$\beta = \frac{3 + 2K}{1 + 2K}. \tag{15}$$

Equations (13) and (15) thus yield the tricritical line in the three-dimensional space spanned by (T, Δ, K). This line is stable as long as $C_c > 0$, and it terminates at a fourth-order critical point at which $C_c = 0$. On the tricritical line, where $A_c = B_c = 0$, C_c takes the form

$$C_c = \frac{\beta^5}{1620(\beta - 1)^2}(9 + 2\beta - \beta^2). \tag{16}$$

It vanishes at $\beta^2 - 2\beta - 9 = 0$. This equation, together with (13) and (15), yields the fourth-order critical point

$$\begin{aligned} T^* &= (1 + \sqrt{10})^{-1} \approx 0.2402, \\ K^* &= (3T^* - 1)/[2(1 - T^*)] \approx -0.1838, \\ \Delta^* &= T^*\left\{K^* + \ln\left[\frac{2(1 - T^*)}{T^*}\right]\right\} \approx 0.399. \end{aligned} \tag{17}$$

In order to complete the phase diagram one has to find the global minimum of the free energy $\tilde{f}(\beta, x, y)$, which is done numerically. In Fig. 2 the phase diagram in the (Δ, T) plane for fixed $K < K^*$ is displayed. One finds in the figure both

ordered and disordered phases separated by continuous (solid) and first-order transition (dashed) lines. The critical line terminates on the first-order surface at a critical end point denoted by P_2^C. The first-order line is composed of two segments, one separating a paramagnetic from a ferromagnetic phase, and the other separating two magnetically ordered phases m_1 and m_2, with $m_1 \neq m_2$. This segment terminates at a critical point, labeled as P_3^C. The two magnetically ordered phases are characterized also by different quadrupole moments q. This can be seen from Eq. (10) (recall that at the minimum of the free energy, x and iy correspond to the equilibrium magnetization and quadrupole moment, respectively): at given β, a jump in x implies a jump in y.

III. MICROCANONICAL ANALYSIS

In order to analyze the phase diagram of the model within the microcanonical ensemble we note that the energy of any microscopic configuration can be expressed in terms of only two parameters: the total number of up-spins N_+ and total number of down-spins N_-. The number of spins taking the value $S = 0$, N_0, is simply related to N_+ and N_- by $N_+ + N_- + N_0 = N$. The energy (1) is thus given by

$$E = \Delta Q - \frac{1}{2N}M^2 - \frac{K}{2N}Q^2, \tag{18}$$

where $M = N_+ - N_-$ and $Q = N_+ + N_-$, which are the magnetic and quadrupole moments, respectively. To calculate the entropy associated with the macroscopic state defined by M and Q, one has to enumerate the possible microscopic configurations W specified by the values of N_+, N_-, and N_0. This is given by

$$W = \frac{N!}{N_+!N_-!N_0!}. \tag{19}$$

In the large N limit the entropy $S = \ln W$ is

$$S = -N[(1-q)\ln(1-q) + \tfrac{1}{2}(q+m)\ln(q+m) + \tfrac{1}{2}(q-m)\ln(q-m) - q\ln 2], \tag{20}$$

where $m = M/N$ and $q = Q/N$ are the single-site magnetic and quadrupole moments, respectively. The entropy at equilibrium can now be obtained by maximizing Eq. (20) at a fixed energy value E.

Expressing the single site energy $\epsilon = E/N$ in terms of the single-site macroscopic quantities m and q, Eq. (18) becomes

$$q^2 - 2\frac{\Delta}{K}q + \frac{2\epsilon}{K} + \frac{m^2}{K} = 0. \tag{21}$$

This allows a solution for q in terms of m and ϵ:

$$q_\pm = \frac{\Delta}{K} \pm \sqrt{\left(\frac{\Delta}{K}\right)^2 - \frac{2\epsilon}{K} - \frac{m^2}{K}}. \tag{22}$$

For given values of the parameters Δ and K and of the magnetization m, the energy ϵ must be in a range such that the expression under square root is not negative. For $K < 0$, the only acceptable solution is q_+, since q_- is negative. Substituting the solution for q_+ in the expression for the entropy (20), one obtains the single-site entropy $S/N = \tilde{s}_+(\epsilon, m)$ as a function of ϵ and m. The equilibrium entropy corresponds to the global maximum of $\tilde{s}_+(\epsilon, m)$ as a function of m, i.e., $s_+(\epsilon) = \max_m[\tilde{s}_+(\epsilon, m)]$.

In order to find the critical and multicritical surfaces of the phase diagram we expand the entropy $\tilde{s}_+(\epsilon, m)$ around the paramagnetic phase $m = 0$. The expansion takes the form

$$\tilde{s}_+(\epsilon, m) = s_0 + A_m m^2 + B_m m^4 + C_m m^6 + D_m m^8 + O(m^{10}) + \cdots, \tag{23}$$

where s_0 is the zero magnetization entropy:

$$s_0 = -(1-z_+)\ln(1-z_+) - z_+\ln z_+ + z_+\ln 2 \tag{24}$$

with $z_+ = q_+(m=0)$. The expansion coefficients are given by

$$\begin{aligned}
A_m &= -a\ln\frac{2(1-z_+)}{z_+} - \frac{1}{2z_+},\\
B_m &= -Ka^3\ln\frac{2(1-z_+)}{z_+} - \frac{a^2}{2z_+(1-z_+)} - \frac{a}{2z_+^2} - \frac{1}{12z_+^3},\\
C_m &= -2K^2a^5\ln\frac{2(1-z_+)}{z_+} - \frac{Ka^4}{z_+(1-z_+)} + \frac{a^3(2z_+-1)}{6z_+^2(1-z_+)^2} - \frac{Ka^3}{2z_+^2} - \frac{a^2}{2z_+^3} - \frac{a}{4z_+^4} - \frac{1}{30z_+^5},\\
D_m &= -5K^3a^7\ln\frac{2(1-z_+)}{z_+} - \frac{5K^2a^6}{2z_+(1-z_+)} + \frac{Ka^5(2z_+-1)}{2z_+^2(1-z_+)^2} - \frac{a^4(1-3z_++3z_+^2)}{12z_+^3(1-z_+)^3} - \frac{K^2a^5}{z_+^2}\\
&\quad - \frac{Ka^4}{z_+^3} - \frac{a^3}{2z_+^4} - \frac{Ka^3}{4z_+^4} - \frac{a^2}{2z_+^5} - \frac{a}{6z_+^6} - \frac{1}{56z_+^7},
\end{aligned} \tag{25}$$

where the subscript m denotes the microcanonical coefficients and

$$a = \mathrm{sgn}(K)(4\Delta^2 - 8K\epsilon)^{-\frac{1}{2}}. \tag{26}$$

The critical surface in the (ϵ, Δ, K) space is obtained at $A_m = 0$ with $B_m < 0$. To obtain the expression giving $A_m = 0$ we start from the microcanonical inverse temperature, given by

$$\beta = \frac{\partial\tilde{s}_+}{\partial\epsilon} = \ln\left[\frac{2(1-q_+)}{\sqrt{q_+^2 - m^2}}\right]\frac{\partial q_+}{\partial\epsilon}, \tag{27}$$

where m takes the value which maximizes $\tilde{s}_+(\epsilon, m)$. On the critical line, where $m = 0$, this expression becomes

$$\beta = \frac{\partial s_0}{\partial\epsilon} = -2a\ln\frac{2(1-z_+)}{z_+}. \tag{28}$$

Substituting this equation in $A_m = 0$ one obtains $z_+ = 1/\beta$. Inserting this into Eq. (28) we have $\beta = \frac{1}{2}e^{-\frac{\beta}{2a}} + 1$. On the other hand, from the definition of a given in Eq. (26) we obtain $\beta/(2a) = K - \beta\Delta$. So at the end $A_m = 0$ is expressed by

$$\beta = \tfrac{1}{2}\exp[\beta\Delta - K] + 1, \tag{29}$$

Note that the expression of the critical surface is the same as the one obtained for the canonical ensemble, as expected [7,22].

Similarly the tricritical line marking the termination of the critical surface, is obtained at $A_m = B_m = 0$, with $C_m < 0$.

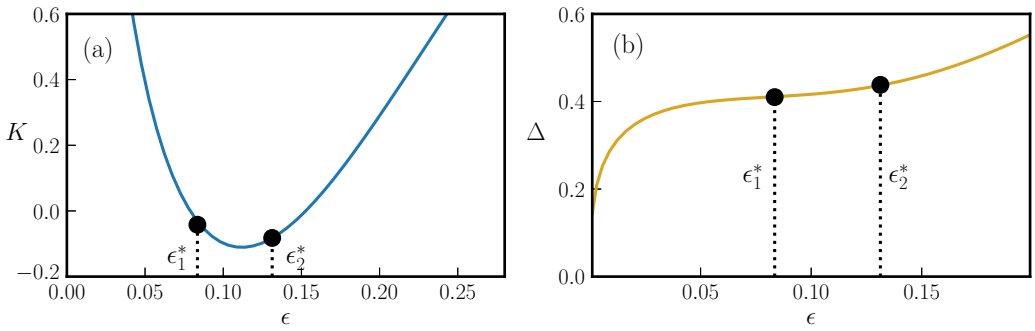

FIG. 3. The tricritical line obtained from the microcanonical analysis by solving for $A_m = B_m = 0$ [see Eq. (23)], plotted in both the (ϵ, K) plane (a) and (ϵ, Δ) plane (b). Solutions for the fourth-order critical points, $\epsilon_1^* \approx 0.0835$ and $\epsilon_2^* \approx 0.1313$, are indicated by black dots.

These equations can be solved, and the tricritical line in the $(\epsilon,\ \Delta,\ K)$ space can be expressed in terms of the parameter β as

$$K(\beta) = \frac{3-\beta}{2\beta-2},$$
$$\Delta(\beta) = [K(\beta) + \ln(2\beta-2)]\beta^{-1},$$
$$\epsilon(\beta) = \frac{\Delta(\beta)}{2\beta} + \frac{\ln(2\beta-2)}{\beta^2\Delta(\beta)}. \tag{30}$$

In Fig. 3 we represent the tricritical line by plotting K [Fig. 3(a)] and Δ [Fig. 3(b)] as a function of ϵ.

The tricritical line terminates at the fourth-order critical point which is obtained at $A_m = B_m = C_m = 0$ with $D_m < 0$. The three constraints yield a point in the parameter space. To find the solution to these equations we plot (Fig. 4) the coefficients C_m and D_m as a function of ϵ, along the tricritical line. One can see that there are two solutions corresponding to two energy values, $\epsilon_1^* \approx 0.0835$ and $\epsilon_2^* \approx 0.1313$, at which the sixth-order coefficient C_m in the expansion vanishes. At both solutions the eighth-order coefficient is $D_m < 0$ indicating that both are locally stable solutions. We will see below that the only solution which corresponds to a global maximum of the entropy is ϵ_2^*. The other solution is preempted by a global maximum away from $m = 0$. Thus the fourth-order critical point of the microcanonical ensemble takes place at

$$\epsilon_2^* \approx 0.1313,\quad \Delta_2^* \approx 0.4369,\quad K_2^* \approx -0.0828, \tag{31}$$

which corresponds to $T^* \approx 0.2924$. Comparing these values with the fourth-order point found from the canonical calculation (17) shows that that the two differ from each other.

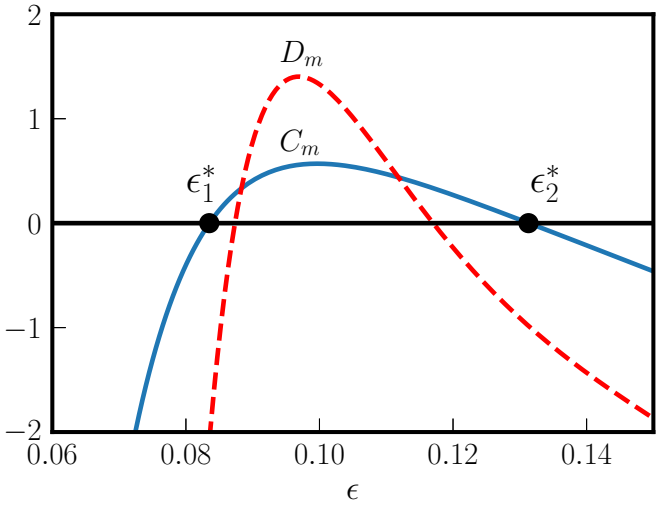

FIG. 4. The values of the coefficients C_m and D_m [see Eq. (23)], plotted as a function of the energy per particle ϵ, for the parameter values corresponding to the tricritical line ($A_m = B_m = 0$). The fourth-order critical points can be read out from the figure, corresponding to $C_m = 0$ and $D_m < 0$, with values $\epsilon_1^* \approx 0.0835$ and $\epsilon_2^* \approx 0.1313$.

To complete the phase diagram one has to determine the first-order surfaces of the model. This is done by numerically finding the global maximum of the entropy. Before analyzing the detailed phase diagram near the fourth-order critical point, which will be presented in the next section, let us display the global features of the phase diagram. A schematic phase diagram in the (Δ, ϵ) plane for some values of K is given in Fig. 5. For $K > K_2^*$, the phase diagram consists of a transition line from a paramagnetic to a ferromagnetically ordered phase, which changes character from second-order to first-order at a tricritical point. At $K = K_2^*$ the tricritical point becomes a fourth-order point, and for $K < K_2^*$ the first-order line extends into the magnetically ordered phase, indicating a transition between two ordered phases, and the second-order line terminates at a critical end point. Also in the microcanonical ensemble, the two ordered phases between which a first-order transition takes place are characterized by different magnetization and a different quadrupole moment. This can be seen from Eq. (22): at given ϵ, a jump in m implies a jump in q_+. It is evident that the microcanonical (Δ, ϵ) phase diagram is qualitatively similar to the canonical (Δ, T) as discussed in the preceding section. In particular, the qualitative features of the canonical (Δ, T) phase diagram for K larger, equal, and smaller than K^* are, respectively, similar to those shown in Fig. 5 concerning the (Δ, ϵ) phase diagram for K larger, equal, and smaller than K_2^*. In the next section we consider the detailed microcanonical phase diagram near the fourth-order critical point and present it in the (T, Δ, K) space, where the comparison with the canonical phase diagram reveals the inequivalence between the two ensembles.

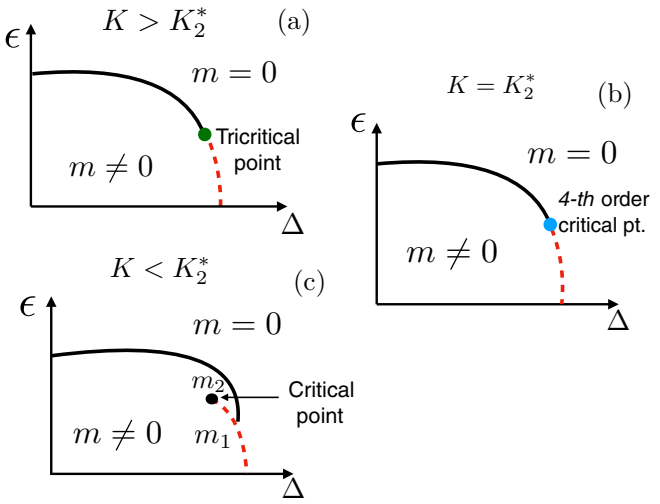

FIG. 5. Schematic microcanonical phase diagram near to the fourth-order critical point. The panels show the phase diagrams in the (Δ, ϵ) plane for fixed K values. Panel (a) displays a $K > K_2^*$ plane where the ordered phase ($m \neq 0$) and the disordered phase ($m = 0$) are separated by two transition line segments: a continuous (solid) and a first-order (dashed) transition line that merge at the tricritical point. Panel (b) corresponds to $K = K_2^*$. It is similar to panel (a); however, the two segments of the transition line join at a fourth-order point rather than a tricritical one. In panel (c), which corresponds to $K < K_2^*$ the two segments of the transition line join at a critical end point. The first-order transition line extends into the ordered phase indicating transitions between two different ordered phases with magnetization values m_1 and m_2.

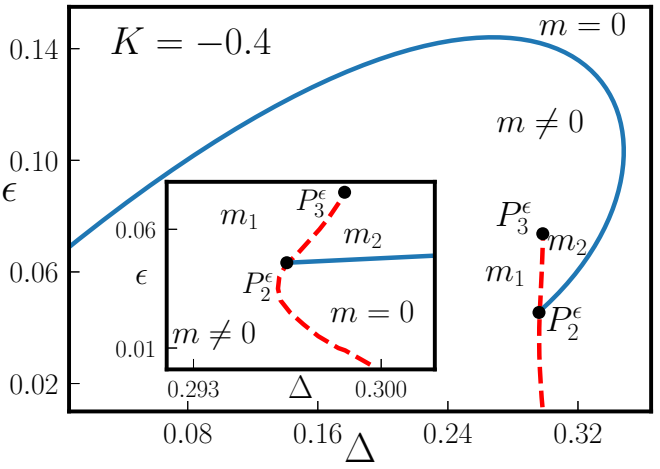

FIG. 6. The microcanonical phase diagrams in the (Δ, ϵ) plane for a fixed value of $K = -0.4$. The locus of continuous transition points in the plane is plotted as a solid line (in blue) and the first-order locus with dashed line (in red). The first-order transition line is seen to extend into the ordered phase, indicating a transition between two ordered phases. The continuous transition line terminates at P_2^ϵ ($\Delta \approx 0.2966$, $\epsilon \approx 0.0459$). The critical point P_3^ϵ ($\Delta \approx 0.2987$, $\epsilon \approx 0.075$) marks the termination of the first-order line in the ordered phase. The inset shows a zoomed-in plot near the region in the phase diagram close to the first-order transition, indicating the reentrant behavior in the ordered phase, as the energy is varied at fixed Δ.

IV. MICROCANONICAL PHASE DIAGRAM NEAR THE FOURTH-ORDER POINT

In this section, we consider the microcanonical phase diagram near to the fourth-order point. In particular we discuss the phase diagram for $K = -0.4 < K_2^*$ first in the (Δ, ϵ) plane, and then in the (Δ, T) plane. The detailed (Δ, ϵ) phase diagram is plotted in Fig. 6. It shows a first-order line which extends into the magnetically ordered phase and a critical line terminating at a critical end point, as discussed in the preceding section. The inset of Fig. 6, which zooms onto the region where the two lines meet, shows that the first-order line curves backward, resulting in reentrant transitions as the energy is increased for some narrow range of Δ. This will result in some interesting features of the phase diagram when plotted in the (Δ, T) plane.

In order to compare the phase diagrams of the two ensembles we now replot the (Δ, ϵ) phase diagram of Fig. 6 in the (Δ, T) plane. Since some of the interesting features of the phase diagram show up in a rather narrow range of the parameters, we first plot in Fig. 7(a) a schematic phase diagram on a broader scale. A zoomed-in nonschematic plot focused on the more interesting region of the phase diagram is given in Fig. 7(b). In the microcanonical ensemble, a first-order transition is characterized by a temperature discontinuity. Thus in the figure one notices that the first-order transition is represented by two lines which give the two temperature values at the transition.

To get some insight into the phase diagram it is convenient to consider the caloric curve and plot the temperature as a function of ϵ at fixed Δ. This is done for two representative values of Δ: (1) $\Delta = 0.2972$, for which two first-order transitions and one second-order transition take place, and (2) $\Delta = 0.2964$, where the second-order transition is absent. The first-order transitions have to do with the curved (reentrant) shape of the first-order line in the (Δ, T) plane. The plots, Figs. 8(a) and 8(b), show $T(\epsilon)$ for the two respective values of Δ.

Consider first Fig. 8(a). At low energy (and low temperature) the $T(\epsilon)$ curve corresponds to a magnetically ordered state. As the energy increases the temperature undergoes a first-order transition into a paramagnetic phase in which the temperature drops discontinuously from a_1 to a_2. At a higher value of the energy a second-order transition takes place at $T = a_3$, where the system becomes magnetically ordered again. By increasing the energy even further, the other first-order transition into a magnetically ordered state with a different magnetization is reached, in which the temperature drops from $T = a_4$ to $T = a_5$. In Fig. 8(b) the corresponding behavior for the lower value of Δ is displayed. Here no second-order transition takes place, and there are two first-order transitions: one is a transition from the magnetically ordered state to the paramagnetic state at a low temperature, followed by a reentrant transition from the paramagnetic state to the magnetically ordered one at a higher temperature. The corresponding temperature drops are from b_1 to b_2 and from b_3 to b_4, respectively. By considering similar curves at other values of Δ one finds that for Δ corresponding to the point P_1^{MC} ($\Delta \approx 0.2961$, $T \approx 0.1244$) in Fig. 7(b) the two

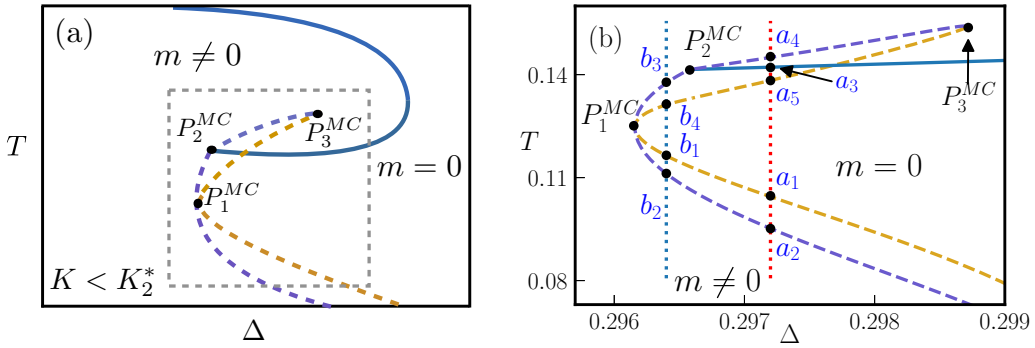

FIG. 7. (a) Schematic phase diagram in the (Δ, T) parameter space with fixed value of $K < K_2^*$ to show the relevant region in the plane where the transition is observed. (b) The nonschematic phase diagram is plotted for $K = -0.4$; this is an enlarged version of a section of the phase diagram [specified by the gray dashed square displayed in panel (a)]. In both plots, the continuous transition line is shown as a solid curve and the first-order transition lines as dashed curves. The label P_1^{MC} denotes the point in the parameter space, where the discontinuity in temperature vanishes. Furthermore, P_2^{MC} represents the point at which the continuous transition line joins the first-order line, and P_3^{MC} is the critical point, where the first-order line terminates. The two vertical lines in panel (b) indicate fixed Δ lines, $\Delta = 0.2972$ (red dotted line) and $\Delta = 0.2964$ (blue dotted line) along which the temperature profile is plotted as a function of ϵ in Fig. 8. The labels $\{a_i\}$ and $\{b_i\}$ correspond to the various transition points along the respective lines.

first-order transitions merge into a single continuous transition where no discontinuity takes place. At a higher value of Δ, corresponding to that of P_3^{MC} ($\Delta \approx 0.29871$, $T \approx 0.1540$) in Fig. 7(b), the first-order transition between the two ordered phases terminates at a critical point, and no such transition exists at higher values of Δ.

To compare the canonical and microcanonical phase diagrams, we superimpose in Fig. 9 the two (Δ, T) phase diagrams for $K = -0.4$. As is clear from the figure the canonical continuous transition line from the disordered phase coincide with the microcanonical one. The first-order lines separating the disordered and the ordered phases are different in the two ensembles, but they remain close to each other. The critical end points in the two phase diagrams are distinct, with ($\Delta \approx 0.2966$, $T \approx 0.1419$) at the canonical point P_2^C, and ($\Delta \approx 0.2972$, $T \approx 0.1412$) at the microcanonical one P_2^{MC}. The two points are very close to each other. Note that in the microcanonical case the first-order line exhibits a discontinuity in its slope at the critical end point, a feature which is absent in the canonical line, whose slope is continuous at the corresponding critical end point. The zoomed-in plot on the transition lines within the ordered phase shows that the canonical first-order line terminates at a critical point P_3^C with ($\Delta \approx 0.29873$, $T \approx 0.1544$) which is close to but distinct from the microcanonical one P_3^{MC} located at ($\Delta \approx 0.29871$, $T \approx 0.1540$).

The different phases that we observe along the caloric curve (see Fig. 8) correspond to the values of m at which the entropy function $\tilde{s}_+(\epsilon, m)$ is maximized. This is illustrated by plotting $\tilde{s}_+(\epsilon, m)$ as a function of m for given values of Δ as ϵ is changed. In Fig. 10 we show the plots for $\tilde{s}_+(\epsilon, m)$ for the same values of Δ considered earlier. Due to symmetry between m and $-m$, it is sufficient to consider the positive domain of m. The left panels of Fig. 10 are for $\Delta = 0.2972$. As also denoted in Fig. 8(a), for small values of ϵ, $\tilde{s}_+(\epsilon, m)$ maximizes at nonzero m. At higher values of ϵ the maximum changes discontinuously to $m = 0$ [indicated by the discontinuity in T in Fig. 8(a)] corresponding to the intermediate disordered phase. As ϵ is increased to larger values, a continuous transition to an ordered phase (denoted by m_2) takes place, followed by a first-order transition to a different magnetically ordered phase (denoted by m_1). A closely similar profile is observed for $\Delta = 0.2964$ as seen in the right panels of Fig. 10. However, it lacks the continuous transition for intermediate values of ϵ but displays only two first-order transitions [also shown in Fig. 8(b)].

V. CONCLUSIONS

In this paper we studied the microcanonical phase diagram of the infinite range Blume-Emery-Griffiths model for negative biquadratic exchange $K < 0$, where the canonical phase diagram has been shown to exhibit a fourth-order critical point. Studying the phase diagram of a model near its higher-order critical point is of particular interest since, as usual, each type of high-order critical point displays distinct characteristic features of the phase diagram around it. These features tend to persist in quite a broad range of the model parameter space. The study of the high-order critical point of a model thus provides valuable information about its global phase diagram.

We find that like the canonical phase diagram, the microcanonical phase diagram exhibits a fourth-order critical point at different coordinates (T, Δ, K) compared with the canonical one. This enables one to compare the two phase diagrams around this point, as is seen in Fig. 2 and Fig. 7. In the vicinity of the microcanonical fourth-order point the transition from the paramagnetic to the ferromagnetic phase can be either continuous or first-order. The first-order transition extends into the ferromagnetic phase, thus separating two different magnetically ordered phases. This transition surface is curved and leads to reentrant transitions as the energy is varied keeping the parameters of the model (Δ, K) fixed. For example, depending on these parameters, as one increases the energy, one may find a sequence of three phase transitions: a first-order transition from $m \neq 0$ to $m = 0$, followed by a continuous transition to a phase with $m \neq 0$ and then followed by another transition separating two magnetically ordered phases. For certain other parameter values the continuous transition is absent, and one encounters a sequence of two

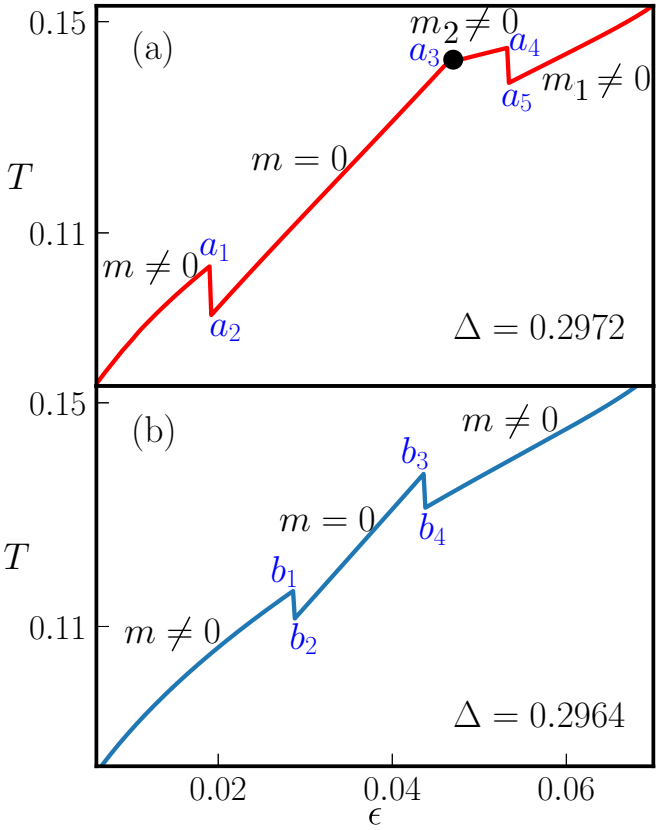

FIG. 8. The temperature profile (caloric curve) for fixed values of $K = -0.4$ for (a) $\Delta = 0.2972$ and (b) $\Delta = 0.2964$ as a function of ϵ. In panel (a), the discontinuities marked by a_1a_2 and a_4a_5 correspond to first-order transitions and a_3 to the continuous transition point. The labels m_1 and m_2 correspond to two values of the magnetization order parameter. In panel (b), the discontinuities b_1b_2 and b_3b_4 correspond to first-order transitions. Equivalent points in the $T - \Delta$ phase diagram [Fig. 7(b)] are marked by the same label for comparison.

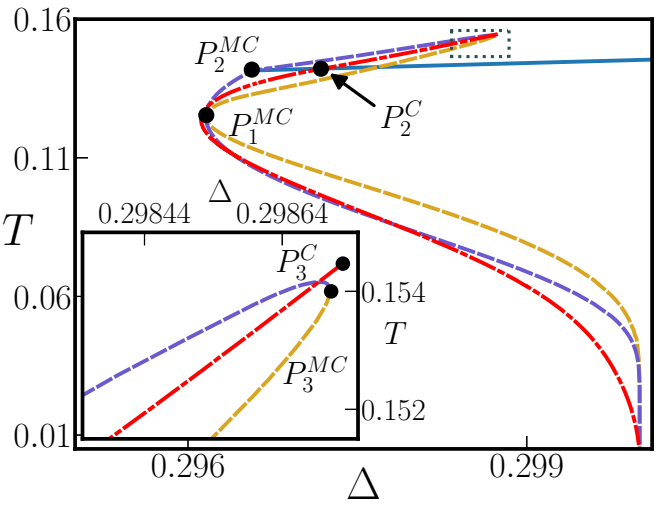

FIG. 9. The canonical and microcanonical (Δ, T) for $K = -0.4 < K_2^*$ superimposed. The canonical first-order line is shown as dot-dashed (red) while the corresponding microcanonical transition is represented by dashed lines. The continuous transition line (solid blue line) terminates at P_2^C (canonical) and at P_2^{MC} (microcanonical) in the two ensembles. The inset shows the enlarged version of the region (dotted square in the main plot) where the first-order transition terminates within the ordered phase at a critical point. In the inset the microcanonical and canonical critical points are labeled as P_3^{MC} and P_3^C, respectively.

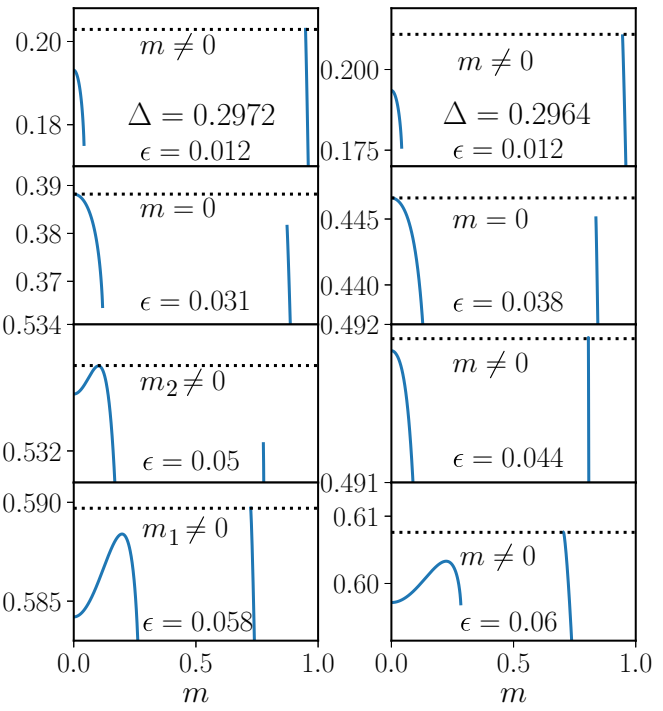

FIG. 10. The entropy function $\tilde{s}_+(\epsilon, m)$ plotted as a function of m for $K = -0.4$ and for $\Delta = 0.2972$ (left panels) and $\Delta = 0.2964$ (right panels), for different values of ϵ. In the left (right) panels each plot represents the profile of $\tilde{s}_+(\epsilon, m)$ in the different phases highlighted in Fig. 8(a) [(b)] as one varies ϵ at fixed values of $\Delta = 0.2972$ [$\Delta = 0.2964$]. In the plots, the maxima of the finite m branch (the branch on the right) in $\tilde{s}_+(\epsilon, m)$ are not visible but can be seen as we zoom in.

first-order transitions. At the first-order transitions the temperature changes discontinuously. This rich phase diagram is quite different from its canonical counterpart, including the presence of singular points of first-order transition without a temperature discontinuity.

The difference in the location of the fourth-order critical point between the two ensembles, in particular with $K_2^* \approx -0.0828$ in the microcanonical case and $K^* \approx -0.1838$ in the canonical case, has the consequence that the (Δ, T) [or (Δ, ϵ)] phase diagram for a K value between K^* and K_2^* presents a tricritical point in the canonical ensemble, while it has a critical end point, together with two different magnetically ordered phases, in the microcanonical ensemble. This is another marked manifestation of ensemble inequivalence.

A closely related model to (1) has been studied in Ref. [20] where the BEG model with nearest-neighbor couplings (both J and K) has been considered within the mean-field approximation in the canonical ensemble. While for positive biquadratic exchange $K > 0$ the model is equivalent to the model considered in the present study and yields the same phase diagram as that of (1), for $K < 0$ the model exhibits other types of order besides the ferromagnetic one.

In particular, for negative and large K, other phases with ferrimagnetic or antiquadrupolar order have been observed. The phase diagram in this domain becomes rather complex with a variety of transitions between the different ordered phases. It would be of interest to extend the present study of the microcanonical phase diagram in the large and negative K regime of the model studied in Ref. [20] and compare it with the canonical one.

ACKNOWLEDGMENTS

We thank N. Defenu for discussions. Support by a research grant from the Center for Scientific Excellence at the Weizmann Institute of Science is gratefully acknowledged. A.C. acknowledges financial support from INFN (Istituto Nazionale di Fisica Nucleare) through the projects DYNSYSMATH and ENESMA.

[1] A. Campa, T. Dauxois, D. Fanelli, and S. Ruffo, *Physics of Long-Range Interacting Systems* (Oxford University Press, Oxford, 2014).
[2] T. Dauxois, S. Ruffo, E. Arimondo, and M. Wilkens, editors, *Dynamics and Thermodynamics of Systems with Long-Range Interactions*, Lecture Notes in Physics Vol. 602 (Springer, New York, 2002).
[3] P.-H. Chavanis, in *Dynamics and Thermodynamics of Systems with Long-Range Interactions*, edited by T. Dauxois, S. Ruffo, E. Arimondo, and M. Wilkens, Lecture Notes in Physics Vol. 602 (Springer, New York, 2002), p. 208.
[4] T. Padmanabhan, Phys. Rep. **188**, 285 (1990).
[5] L. D. Landau and E. M. Lifshitz, *Electrodynamics of Continuous Media* (Pergamon Press, Oxford, 1960).
[6] D. R. Nicholson, *Introduction to Plasma Theory* (Krieger Publishing, Malabar, FL, 1992).
[7] A. Campa, T. Dauxois, and S. Ruffo, Phys. Rep. **480**, 57 (2009).
[8] F. Bouchet, S. Gupta, and D. Mukamel, Physica A **389**, 4389 (2010).
[9] T. Misawa, Y. Yamaji, and M. Imada, J. Phys. Soc. Jpn. **75**, 064705 (2006).
[10] F. Borgonovi, G. L. Celardo, M. Maianti, and E. Pedersoli, J. Stat. Phys. **116**, 1435 (2004).
[11] D. Mukamel, S. Ruffo, and N. Schreiber, Phys. Rev. Lett. **95**, 240604 (2005).
[12] D. Lynden-Bell, Mon. Not. R. Astron. Soc. **136**, 101 (1967).
[13] P.-H. Chavanis, J. Sommeria, and R. Robert, Astrophys. J. **471**, 385 (1996).
[14] V. Latora, A. Rapisarda, and S. Ruffo, Phys. Rev. Lett. **83**, 2104 (1999).
[15] Y. Y. Yamaguchi, J. Barré, F. Bouchet, T. Dauxois, and S. Ruffo, Physica A **337**, 36 (2004).
[16] M. Blume, V. J. Emery, and R. B. Griffiths, Phys. Rev. A **4**, 1071 (1971).
[17] D. Mukamel and M. Blume, Phys. Rev. A **10**, 610 (1974).
[18] S. Krinsky and D. Mukamel, Phys. Rev. B **11**, 399 (1975).
[19] J. Lajzerowicz and J. Sivardière, Phys. Rev. A **11**, 2079 (1975).
[20] W. Hoston and A. N. Berker, Phys. Rev. Lett. **67**, 1027 (1991).
[21] V. V. Hovhannisyan, N. S. Ananikian, A. Campa, and S. Ruffo, Phys. Rev. E **96**, 062103 (2017).
[22] J. Barré, D. Mukamel, and S. Ruffo, Phys. Rev. Lett. **87**, 030601 (2001).
[23] M. Baldovin, Phys. Rev. E **98**, 012121 (2018).
[24] T. M. Rocha Filho, C. H. Silvestre, and M. A. Amato, Commun. Nonlinear Sci. Numer. Simulat. **59**, 190 (2018).